www.czasopisma.pan.pl PAN POLSKA AKADEMIA NAUK www.journals.pan.pl

Arch. Metall. Mater. **68** (2023), 1, 15-20

DOI: https://doi.org/10.24425/amm.2023.141466

ZHIMING LIU[1], QIANG ZHANG[2], FANGYING LIU[2], HEZHE ZHANG[2*]

COMPARISON OF WEAR RESISTANCE IN POLYCRYSTALLINE AND MONOCRYSTALLINE IRON

In the present research, we used molecular dynamics simulation to determine the effect of cutting parameters on micro-grain boundary structures and Burgers vector distribution in single crystal iron and polycrystalline iron materials. The result showed that the destruction of the lattice in polycrystalline iron caused by the cutting tool was restricted to the contact surface area. In addition, in the precision machining process, a higher refining grain was observed on the iron surface. During the cutting process of single crystal iron, large-scale slip occurred along the <111> crystal direction on the {110} crystal plane. And the slip presented an annular shape.

Keywords: Molecular dynamics; Polycrystalline; Centro symmetric analysis; Abrasive wear

1. Introduction

Iron is the most commonly used metal in industry. In this respect, iron-based alloys are widely used in construction, manufacturing, and in everyday life. In addition to the alloy phase, pure iron is also widely used in industrial production. Because of its excellent plasticity, high purity iron, including industrial pure iron and electrolytic iron, can be stamped into extremely complex shapes using different deep drawing techniques. In addition, it is used in a variety of high-performance and high-density electronic components because of its magnetic properties. In general, pure iron is highly valuable for its applications in aerospace, weapons, energy, and electronics, among other fields [1].

However, since pure iron is extremely soft, many difficulties arise during its processing. Thus, in order to ensure the proper accuracy during surface processing, different problems need to be solved. For example, when cutting pure iron, severe friction in the cutting area and rapid cutting tools cause chip deformation and chip accumulation. These phenomena affect the accuracy during surface processing, also affecting the value of key components in high-precision instruments [2,3]. Therefore, understanding the anti-cutting characteristics of pure iron is of great significance for improving the accuracy in pure iron processing. This will improve the precision rate in finished products containing precision components.

To the best of our knowledge, most research has determined the effects of macro cutting parameters on the machined parts and the influence of different cutting tool materials on machining accuracy and surface characteristics [4]. However, a significant amount of problems have not been deeply studied including: (a) the micro-dynamic behavior, tool variation, and friction on iron surface; (b) changes in crystal structure during the cutting process; (c) iron cutting models at the micro-scale level; (d) the influence of iron grain boundaries on cutting behavior; and (e) iron damage resistance under different microenvironments. In the present investigation, we used molecular dynamics simulation to improve the machining surface accuracy of iron micro-cutting machines.

2. Molecular dynamics model

The micro-cutting process was simulated using the second generation nano-cutting molecular dynamics simulation model [5] proposed by Belak and Stowers. The simulation model was built as shown in Fig. 1. In the model, the material to be cut was divided into three layers: boundary layer, constant temperature layer, and Newton layer. Among them, the boundary layer is located at the edge of the material, which plays a role in fixing the material and reducing the boundary effect. The constant temperature layer is set between the boundary layer and the Newton layer at a given temperature. This layer connects and fixes the atoms at the Newton layer. In addition, it allows the transfer of the heat generated in the process. The Newton layer is set inside

[1] CHINA UNIVERSITY OF MINING AND TECHNOLOGY (BEIJING), BEIJING 100083, CHINA
[2] SHANDONG UNIVERSITY OF SCIENCE AND TECHNOLOGY, QINGDAO 266590, SHANDONG, CHINA

* Corresponding author: 1103070190@qq.com

the constant temperature layer, and its motion characteristics comply with Newton's second motion law. It interacts with the tool material as the processed object [6].

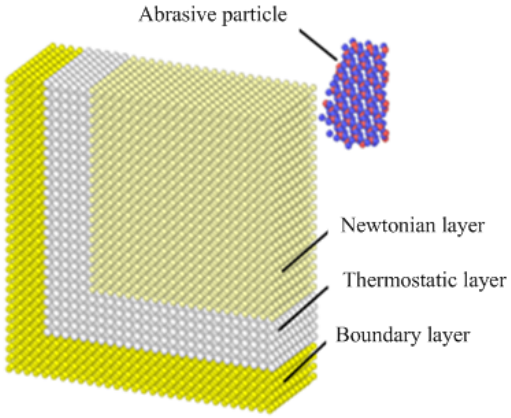

Fig. 1. Single crystal iron cutting model

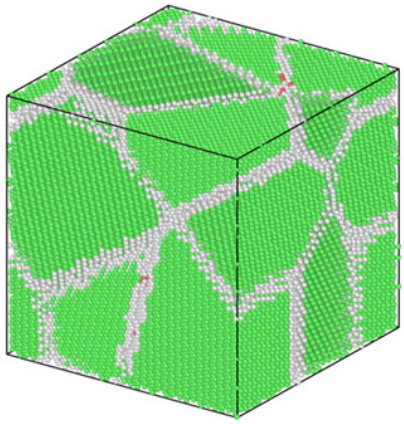

Fig. 2. Polycrystalline iron model

The single-crystal iron structure was built by using an array of body-centered cubic crystal cells with a constant lattice of 2.863. For this purpose, we used the large-scale molecular parallel computing device lamps. As shown in Fig. 2, the polycrystalline iron structure was modeled using the C language program according to the Voronoi polygon method [7]. The size of the structure was 120 Å.

The selection of the potential energy function is closely related to molecular dynamics calculations. If different action potentials are selected, the potential energy surface of the system will have different shapes, and the trajectories of molecular motion and internal motion calculated by molecular dynamics will also be different. Thus, it affects the sampling results and the potential energy of the sampling results. This simulation mainly studies the grinding process of silicon dioxide tool on iron metal. The interaction between Fe atoms assumes the Embedded Atom Method (EAM) potential. EAM potential was first proposed by Daw and baskes [8] according to density functional theory. The central idea is that the binding energy in solid metals can be added to the sum of static interactions of the system as embedded energy. The interaction between Si and O atoms depends not only on the distance between atoms but also on the bonding direction. Therefore, the influence of surrounding atoms must be considered when calculating the interaction between silica atoms [9]. In the present investigation, Tersoff potential was used to describe the interaction between silica. Tersoff potential energy accurately describes the interaction between covalent crystals. The potential energy function between iron and silicon dioxide was described using the Lennard Jones potential, which is called L-J potential, or 6-12 potential. This function was first proposed by John Lennard Jones in 1924 [10] to describe the interaction between two neutral atoms (molecules). The parameters of EAM potential and Morse potential are shown in TABLE 1 and TABLE 2.

TABLE 1

EAM potential function parameters

Parameter	Value	Unit
Number of elements	1	
Element type	Fe	
Atomic number	26	
Nrho	10000	
Drho	$3*10^{-2}$	Ev/Å
Nr	10000	
Dr	$5.3*10^{-2}$	Å
Cutoff	5.3	Å
Lattice constant	2.855324	Å
Lattice type	BCC	
Atomic mass	55.845	u

TABLE 2

Tersoff potential function parameters

Parameter	Silicon atom	Oxygen atom
A (ev)	$1.8308*10^{3}$	$1.88255*10^{3}$
B (ev)	$4.7188*10^{2}$	2.18787*10
λ (nm)$^{-}$	24.7990	41.7108
μ (nm)$^{-}$	17.3222	23.5692
β	$1.1*10^{-6}$	$1.1632*10^{-7}$
n	$7.8734*10^{-1}$	1.04968
c	$1.0039*10^{5}$	$6.46921*10^{4}$
d	16.217	4.11127
h	$-5.9825*10^{-1}$	$-8.45922*10^{-1}$
R (1Å)	2.65	1.85

The simulation system considered fixed boundary conditions in the X-axis and Y-axis and free boundary conditions in the z-axis. In our simulation, the unit time step was set to 1FS (1×10^{-15} s), according to the picosecond vibration frequency of iron atoms. The simulation was divided into two stages. In the first stage, the simulation system was set as NVT ensemble. In order to achieve the low-energy structure of iron atoms, temperature was set at 298 K. For this purpose, we used the Berendsen hot bath temperature control method and conjugate gradient method to reduce the temperature and configuration energy of iron atoms. Later, during the second stage, the system was set as NVE ensemble. Herein, the cutting of metallic iron

was performed using a silicon dioxide tool. In addition, a tool speed and backdraft of 1.5 Å/Fs (150 m/s) and 45 Å, respectively, were selected.

3. Simulation of single crystal iron cutting

The essence of metal cutting deformation is the transformation from local order to the disorder of the crystal under the action of the external force of the cutting tool [11]. In the present research, the centrality of the disordered crystal (CSP) was characterized. During the cutting process, the centrosymmetric parameter identifies whether the atoms are located on the metal surface, as well as different potential defects including vacancies, dislocations, and stacking faults. CSP results are shown in Fig. 3 and Fig. 4.

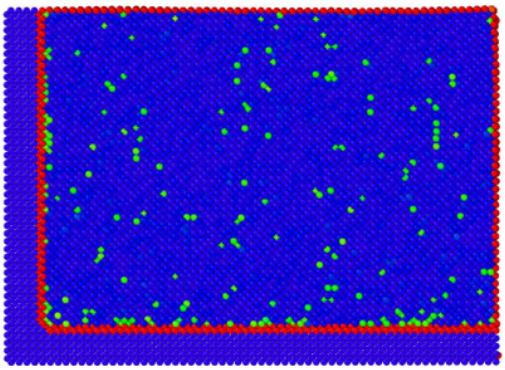

Fig. 3. Centrosymmetric parameter distribution of single crystal iron before cutting

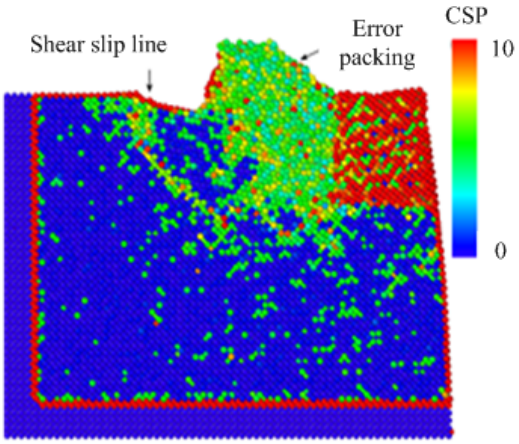

Fig. 4. Centrosymmetric parameter distribution in single crystal iron cutting

According to Fig. 3, the number of atomic trajectory steps was 40000. At this point, the CSP value of most areas was equal to zero. This part of the atomic arrangement displayed a long-range order. That is, the ideal crystal atoms were orderly and periodically arranged according to the spatial lattice points, which belong to the perfect lattice. In the figure, some green atoms are randomly distributed inside the metal in a discrete manner, with CSP values of 5 ~ 6. These atoms displayed high kinetic energy during thermal motion. The excessive kinetic energy causes the atoms to deviate from equilibrium and move to the surrounding lattice to form gap atoms. Every time a gap atom is formed, a vacancy on a relatively low potential energy will be formed to attract surrounding atoms to fill the vacancy. The density of point defects of interstitial atoms and vacancies in the metal is positively correlated with temperature. Thus, it is also called thermal defect. The CSP value of atoms in the red region is about 14 ~ 20. Data indicated that these atoms appear on the Newtonian layer surface at the intersection between the constant temperature layer and the boundary layer, indicating that this part contains surface atoms. Fig. 4 displays the distribution of centrosymmetric parameters of iron along the {100} crystal plane during tool cutting. As this Figure shows, parameters were set up to 110000 steps, a relative speed between the cutting tool and the iron piece of 1.5 Å / Fs (150 m/s), and a pressing depth of the tool of 45 Å. In addition, the cutting was performed horizontally from right to left. Moreover, the atoms in the first deformation zone of the metal presented shear slip along the shear stress direction. As cutting tool moved, some atoms in this area were able to accumulate and rise to the tool surface producing wear debris (top green area). The other part was pressed by the bottom end of the tool forming plastic channels (red area). Fig. 4 also shows a CSP value of 5 in most atomic areas at the front end of the tool movement. Because of tool shear stress, most of the ordered atomic array was lost in this region, where stacking fault and dislocation structures were formed. As a result of the relative tool movement, a large number of these structures were accumulated in the work hardening area at the front end of the tool travel direction. Because of the mutual interaction of dislocation structures, a large number of dislocation entanglement and stacking formed in this area, resulting in the increase of local hardness. Obviously, it is easier to produce dislocations on the metal surface than inside the metal. As Fig. 4 shows, the density of sporadic green areas in the metal was higher than that in Fig. 3, and some of them represent the accumulation of multiple atoms, not a single atom.

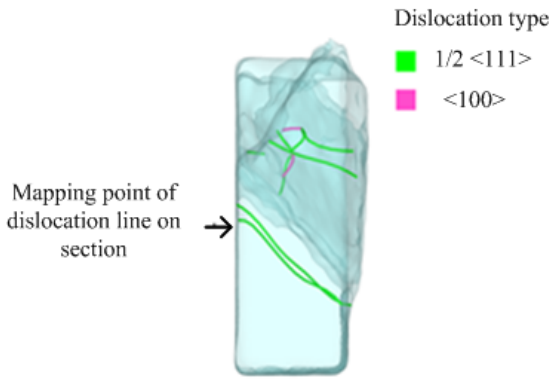

Fig. 5. Burgers vector distribution in single crystal iron

According to the Burgers vector distribution shown in Fig. 5, the scattered green areas indicate the location of edge dislocation lines, which are mainly of the 1 / 2 <111> type with

a slip plane of {110} crystal plane. Fig. 6 presents the crystal defect network diagram and Fig. 7 the centrosymmetric parameter distribution of dislocation atoms. Data in Figs. 6 and 7 indicate that the internal metallic atoms displayed large-scale slips along the crystal plane. In addition, instead of layer-by-layer sliding, the whole block descended forming an annular slip belt. This occurred because the atomic density of the {110} crystal plane in the body-centered cubic structure was higher than that of other crystal planes. In addition, the atomic density in the <111> direction was higher than that in other directions. The highest atomic spacing was observed between the crystal planes with the highest density and crystal direction. Thus, at this point, the smallest atomic binding force and lowest resistance occurred. As a consequence, when the iron piece was subjected to a large enough external force and large-scale deformation, the first slip happened along this direction.

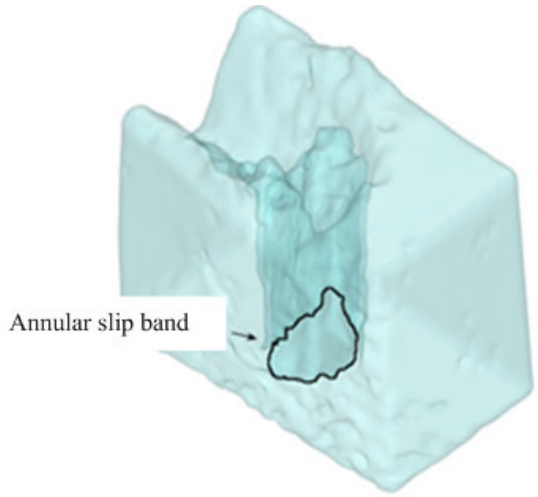

Fig. 6. Defect in single crystal iron

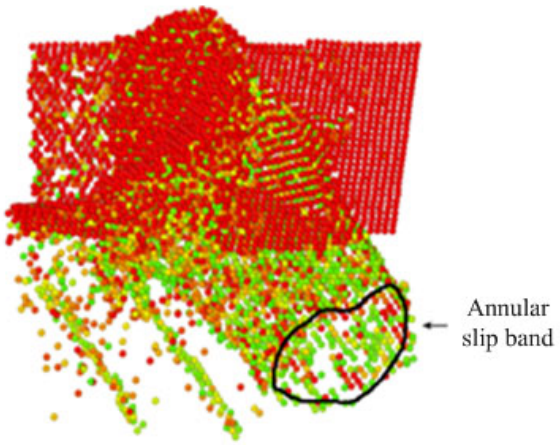

Fig. 7. Symmetric distribution of dislocation centers in single crystal iron

4. Simulation of polycrystalline iron cutting

In molecular dynamics simulation, the Voronoi polygon is the most commonly used method for polycrystalline materials. Voronoi polygon was first proposed by Russian mathematician G.F. Voronoi, and was widely applied in meteorology, geology, crystallography, and urban management. In molecular dynamics simulations, Chen et al. [12] first applied Voronoi method to model nano polycrystalline materials. These researchers compared the actual crystal structure with atomic arrangement, energy distribution, and mechanical characteristics. Their results showed that the properties of Voronoi polycrystals were in good agreement with the actual crystal structure, which verified the reliability of Voronoi polygonal polycrystal model.

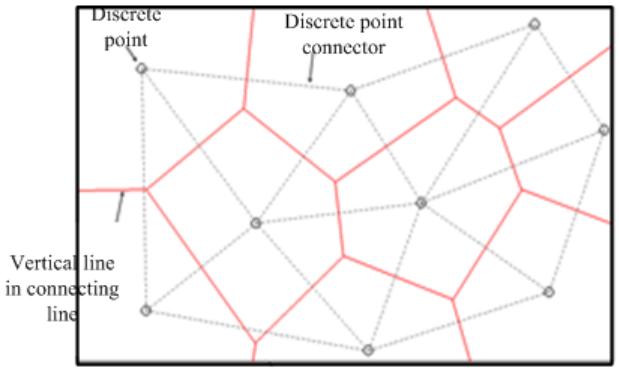

Fig. 8. Voronoi polygon

Because of the existence of internal grain boundaries, polycrystalline iron materials are very different from single crystal materials in terms of in-situ dislocation, nucleation, and their evolution mechanism. After the establishment of the dislocation theory, many dislocation models for grain boundary structures have been studied. Experiments have shown that the small-angle grain boundary is composed of a series of dislocations, while the structure of the large-angle grain boundary is complex. Although some models have been proposed in the past, they have not provided clear details about grain boundary structure. In addition, they have not satisfactorily explained some grain boundary properties. However, it is certain that many complex lattice defects such as vacancies, dislocations, spin errors, and segregation are mixed at the grain boundary. Fig. 9 displays the

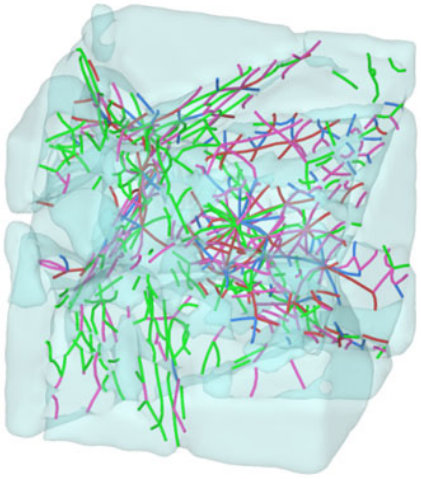

Fig. 9. Symmetrical distribution of dislocation centers in single crystal iron

Boggs vector diagram after relaxation of the polycrystalline iron. As this Figure shows, a variety of dislocation lines were distributed along the curved surface in the polycrystal. The surface distribution of these dislocation lines correspond to the location of the grain boundary.

Subsequently, we analyzed structural changes in polycrystalline and single crystal iron during the cutting process in combination with the central symmetric parameter distribution. During the simulation, we selected a relative tool speed of 1.5 Å/Fs (150 m/s), a horizontal speed to the left along the direction shown in the figure, and a tool pressing depth of 45 Å. As shown in this Figure. the track steps were 110000.

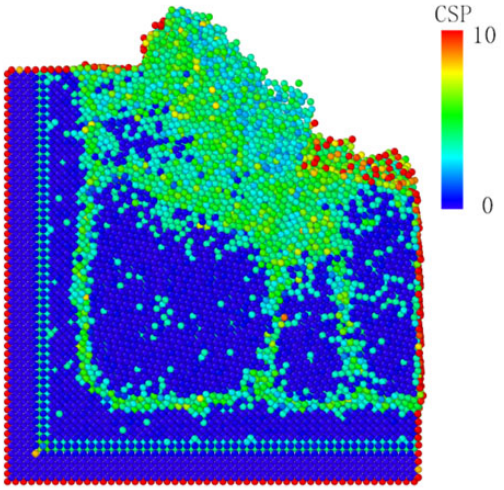

Fig. 10. Symmetric distribution of dislocation centers in single crystal iron

Fig. 10 shows the atoms in the blue region as perfect lattice structures, and the atoms in the green region correspond to defective lattice structures. Data indicated that, with tool movement, the elastic deformation of the grain did not comply with the strain demand. The contact area between the crystal and the cutting tool was plastically deformed along the direction of the tangential force. Some atoms accumulated on the front surface of the tool producing wear debris. The atoms formed protuberances on both sides, which are composed of dislocation and amorphous structures. It was also observed that sporadic green areas were distributed in the grains, and these atoms corresponded to point defects caused by thermal movement. Thus, the distribution of point defects and the formation of wear debris were very similar to those observed during the cutting process of single crystal iron. However, the lattice defects shown in Fig. 11 indicated that, when the same tool size and moving speed were used during the cutting process, polycrystalline iron did not present large-scale slip bands in the same direction as those observed in single crystal structures.

According to our findings, these phenomena occurred because of differences in grain directions in the polycrystalline structure. In addition, no uniform low bond energy in the crystal plane and crystal direction were observed, and the ability of each grain to resist deformation in the same direction was also different. Within the grain, stress caused a uniform deformation, while at the grain boundary, non-uniform deformation occurred. Therefore, large-scale slip bands with the same slip direction were not observed. More importantly, the barrier effect on dislocation propagation within grain boundary prevented the expansion of dislocation within the crystal. Because of different orientations of adjacent grains, atoms in the grain boundary presented lattice variations. These variations caused that atoms at the grain boundary were unable to reach equilibrium and low potential energy. It was also observed that the potential energy barrier formed by lattice elastic distortion caused that grain boundary atoms absorbed more strain energy during elastic deformation. When the dislocation propagated to the grain boundary, the energy of dislocation propagation was absorbed by the grain boundary, resulting in incomplete dislocation propagation in the metal.

5. Conclusion

(1) During the cutting process, the areas of stress concentration in single crystal and polycrystalline iron were the same. These were located on the shear slip area of the metal. The stress concentration in this region induced the shear slip movement of the crystal. The direction of shear slip was

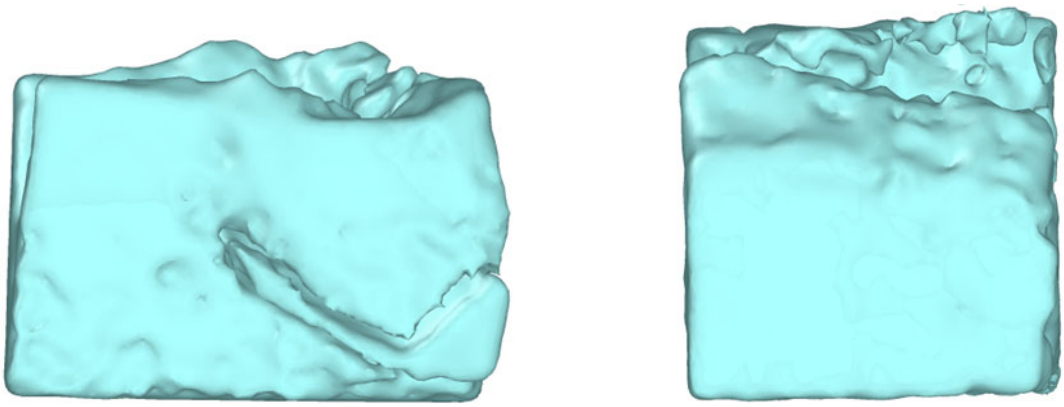

(a) Single crystal iron (b) Polycrystalline iron

Fig. 11. Symmetric distribution of the polycrystalline structure

determined by the direction of shear stress applied by the tool. The shear slip movement in this region was not affected by crystal orientation and grain boundary factors.

(2) During the cutting process of single crystal iron, large-scale slip occurred along the <111> crystal direction on the {110} crystal plane. The slip presented an annular shape. It was concluded that the reason for this phenomenon is that the body-centered cubic structure of iron presented the highest atomic density in the <111> direction of the {110} crystal plane, resulting in the lowest atomic binding force between the crystal plane and the crystal direction. The {110} crystal plane and <111> crystal direction corresponded to the slip plane and slip direction of body-centered cubic lattice iron. When stress caused the large-scale slip in the single crystal structure of BCC lattice iron, deformation first occurred in the slip direction on the slip surface. This was independent of the direction of tool movement and the direction of tool stress application.

(3) Because of different grain orientations, variations in slip surfaces and slip directions were observed in polycrystalline iron. During the cutting process, no large-scale slip was observed. At the same time, a large number of lattice defects on the crystal plane of polycrystalline iron were observed in the Boggs vector diagram. The lattice distortion formed by these lattice defects was able to absorb the expansion of dislocation. It was also observed that the grain boundary reduced the damage caused by the cutting tool. Herein, we demonstrated that the grain boundary diminished the damage caused by cutting tools.

REFERENCE

[1] S.G. Wang, K. Long, Q.G. Long, Refinement of industrial pure iron by deep rolling, JOM **12**, 1247-1250 (2003).

[2] J. Kong, F. Deng, Z.H. Xia, L. Li, Study on chip formation characteristics and influencing factors of pure iron, J. South China University of Technology, Natural Science Edition **44** (12), 7-13 (2016).

[3] J.P. Zhu, Y.F. Yang, J.X. Kong, Research on cutting force and surface roughness during precision cutting of pure iron materials, Manufacturing Technology and Machine Tools **3**, 108-112 +117 (2019).

[4] Q. Zhao, B. Wang, J.Q. Yu, Research on the influence of cutting parameters on machin-ing accuracy of parts, Digital Communication World **11**, 278-279 (2017).

[5] J. Belak, B.B. David, F.S. Irving, Simulation of nanometer-scale deformation of metallic and ceramic surfaces, MRS Bulletin **18**, 55-60 (1993).

[6] H. Wang, Diamond tool wear and C-C atomic bond length, Yanshan University, Master Thesis, 2012.

[7] B. Shan, Z.Z. Chen, R.N. Chen, Scale computational simulation of Materials Science: from basic principle to algorithm implementation, Huazhong University of Science and Technology Press, Wuhan 2015.

[8] M.S. Daw, M.I. Baskes, Embedded-atom method: Derivation and application to impurities, surfaces, and other defects in metals, Phys. Rev. B **29**, 6443-6453 (1984).

[9] D. Chen, Structural modeling of nanocrystalline materials, Comput. Mater. Sci. **3**, 327-333(1995).

[10] Z.W. Fang, The influence of metal cutting deformation on the quality of the machined sur-face, Modern Manufacturing Technology and Equipment **12**, 147-148 (2019).

[11] J.E. Jones, On the Determination of Molecular Fields. I. From the Variation of the Viscosity of a Gas with Temperature, Proc. the Royal Society of London Series A **106**, 441-462 (1924).

[12] Y.L. Zhang, Y. Xu, D. Chen, Several modified forms of Tersoff potential function, Science and Technology Innovation Herald 1**3**, 135-135(2018).